ELSEVIER

Earth and Planetary Science Letters 202 (2002) 495–509

EPSL

www.elsevier.com/locate/epsl

Cathodoluminescence, electron microscopy, and Raman spectroscopy of experimentally shock-metamorphosed zircon

Arnold Gucsik [a], Christian Koeberl [a,*], Franz Brandstätter [b], Wolf Uwe Reimold [c], Eugen Libowitzky [d]

[a] *Institute of Geochemistry, University of Vienna, Althanstrasse 14, A-1090 Vienna, Austria*
[b] *Department of Mineralogy, Natural History Museum, A-1014 Vienna, Austria*
[c] *Impact Cratering Research Group, School of Geosciences, University of Witwatersrand, Johannesburg 2050, South Africa*
[d] *Institute of Mineralogy and Crystallography, University of Vienna, Althanstrasse 14, A-1090 Vienna, Austria*

Received 1 March 2002; received in revised form 30 May 2002; accepted 6 June 2002

Abstract

Thorough understanding of the shock metamorphic signatures of zircon could be the basis for the use of this mineral as a powerful tool for the study of old, deeply eroded, and metamorphically overprinted impact structures and formations. This study of the cathodoluminescence (CL) and Raman spectroscopic signatures of experimentally (20–60 GPa) shock-metamorphosed zircon single crystals contributes to the understanding of high-pressure microdeformation in zircon. For all samples, an inverse relationship between the brightness of the backscattered electron (BSE) signal and the corresponding cathodoluminescence intensity was observed. The unshocked sample shows crosscutting, irregular fractures. The 20 GPa sample displays some kind of mosaic texture of CL brighter and darker domains, but does not exhibit any shock metamorphic features in BSE or CL images. The 40 GPa sample shows a high density of lamellar features, which might be explained by the phase transformation between zircon- and scheelite-structure phases of zircon and resulting differences in the energy levels of the activator elements. The CL spectra of unshocked and shocked (20, 40, and 60 GPa) zircon samples are dominated by narrow emission lines and broad bands in the region of visible light and in the near-UV range. The emission lines result from rare earth element activators and the broad bands might be associated with lattice defects. Raman spectra revealed that the unshocked and 20 GPa samples represent zircon-structure material, whereas the 40 GPa sample yielded additional peaks with relatively high peak intensities, which are indicative of the presence of the scheelite-type high-pressure phase. The 60 GPa sample has a Raman signature that is similar to that of an amorphous phase, in contrast to the observations of an earlier TEM study that the crystalline scheelite-structure phase is stable at this shock pressure. The 60 GPa Raman signature cannot be explained at this stage. The results show a clear dependence of the CL and Raman properties of zircon on shock pressure, which confirm the possible usage of these methods as shock indicators.

Keywords: zircon; deformation; shock metamorphism; cathodoluminescence; phase transitions; Raman spectroscopy

1. Introduction

Cathodoluminescence (CL) is an optical phe-

* Corresponding author. Tel.: +43-1-4277-53110; Fax: +43-1-4277-9531.
E-mail address: christian.koeberl@univie.ac.at (C. Koeberl).

0012-821X/02/$ – see front matter
PII: S0012-821X(02)00754-9

nomenon that is based on the generation of visible radiation through sample excitation by high-energetic electrons (in general, energy of incident beam: 5–25 kV; depth of penetration of a sample: 1–3 μm) [1,2]. Wavelengths of the CL emissions range from the ultraviolet (UV) to the infrared and result from a variety of defects (e.g., various structural imperfections, such as poor ordering, radiation damage) and impurities, such as local presence of rare earth elements (REE ions) in the crystal structure of a mineral [2,3]. According to Boggs et al. [4], the combination of scanning electron microscopy and cathodoluminescence analysis (SEM–CL) may provide better spatial resolution and microcompositional information than standard optical methods.

Zircon is a refractory and weathering-resistant mineral that has been proven useful as an indicator of shock metamorphism in the study of impact structures and formations that are old, deeply eroded, and metamorphically overprinted. Thus, it has advantages compared to quartz or other shock-metamorphosed minerals that have been previously used as impact indicators, but are far less refractory than zircon. On the negative side though, zircon is much less abundant in crustal rocks than other minerals, such as quartz and feldspars, which somewhat diminishes its usefulness as a shock indicator mineral.

Shock-induced microdeformation in zircon has been described in samples from a variety of impact environments, including material from confirmed impact structures [5–7], from the Cretaceous–Tertiary boundary, and from the Upper Eocene impact ejecta layer [6,8,9], as well as in experimentally shock-deformed single-crystal zircon [10,11]. Two different types of shock deformation have been observed: (i) planar microdeformations, and (ii) granular (also called polycrystalline, microcrystalline, *strawberry*) texture. Some effort, especially by transmission electron microscopy (TEM), has been made to determine whether the planar microdeformations discernible at the optical scale in shock-metamorphosed zircon represent bona fide planar deformation features (PDFs), well-known from many other shock-metamorphosed rock-forming minerals [12–14], or whether they represent planar fractures or some other type of microdeformation [15]. To date, this problem has not been solved. Leroux et al. [11] established that, on a nanometer-scale, amorphous phases in the form of planar lamellae were formed in experimentally shocked zircon (e.g., in the 40 GPa sample). However, these authors did not confirm that these microlamellae, resembling PDFs, indeed corresponded to the optically resolved, several μm wide, planar/subplanar microdeformations. Leroux et al. [11] also observed numerous planar fractures and dislocation deformation bands. It is possible that these features could correspond to the optically resolved planar microdeformations.

A granular shock texture in zircon was first observed by Bohor et al. [6] in zircon from the Cretaceous–Tertiary distal impact ejecta layer. Since then, it has been observed in zircon from a number of impact structures ([7,16], and references therein), in zircon from a Late Eocene microkrystite layer, and in tektites [9,17]. Complete breakdown of zircon to baddeleyite, presumably as a result of high-temperature dissociation, has been identified in Libyan Desert Glass and corroborated the impact origin of these enigmatic glasses [18].

Leroux et al. [11] found in their TEM investigations of experimentally shocked zircon that the phase transformation from the zircon structure to a scheelite ($CaWO_4$)-type phase that had been previously observed in shock-metamorphosed zircon by Kusaba et al. [19] was complete at 60 GPa shock pressure. Additionally, Leroux et al. [11] observed 10–20 nm wide PDFs in the 60 GPa sample.

No systematic study of CL properties of progressively shocked zircon crystals has been per-

→

Fig. 1. Optical microscopic (as in the case of images of this type in subsequent figures, taken in plane polarized light) (A) (width of image: 1.1 mm), secondary electron (SE) (B), BSE (C), and CL (D) images of the unshocked zircon sample. The unshocked sample shows individual fractures with widths typically ranging from 5 to 25 μm. For SE, BSE, and CL imaging, the area marked in A was scanned.

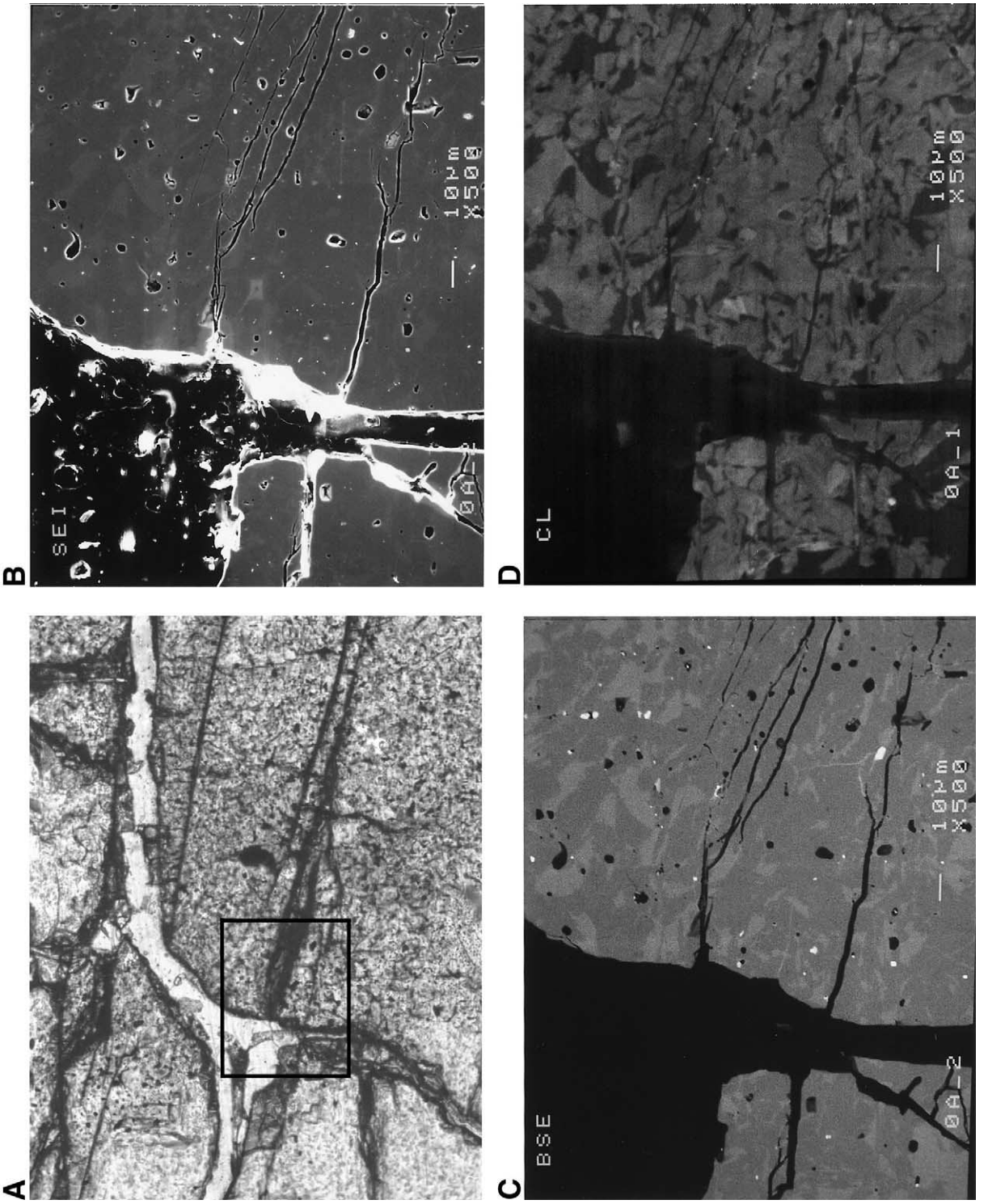
A
B
SEI
10μm
X500
0A-1
C
BSE
10μm
X500
0A-2
D
CL
10μm
X500
0A-1

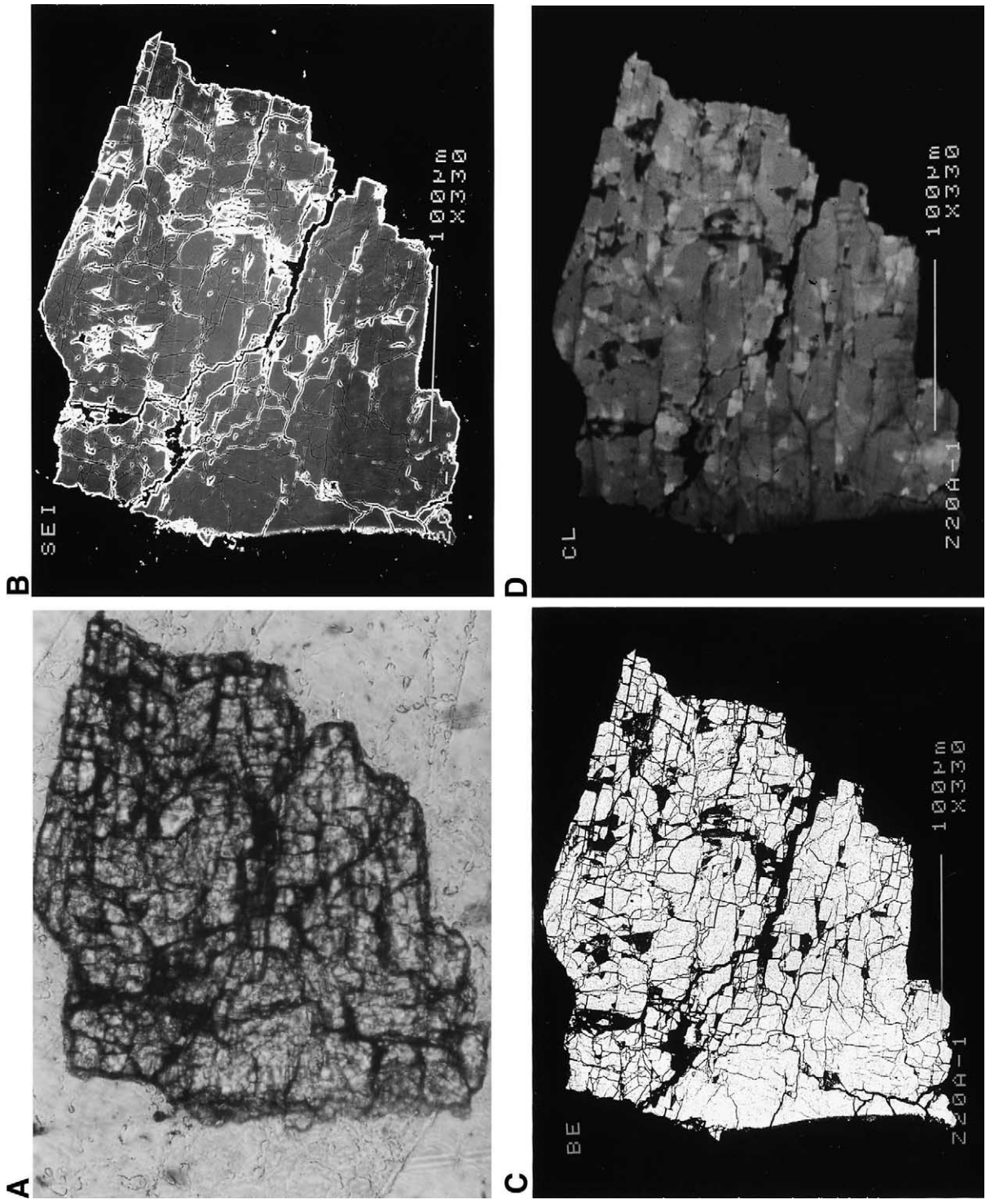
A
B
SEI
100µm
X330
C
BE
100µm
X330
Z204-1
D
CL
100µm
X330
Z204-1

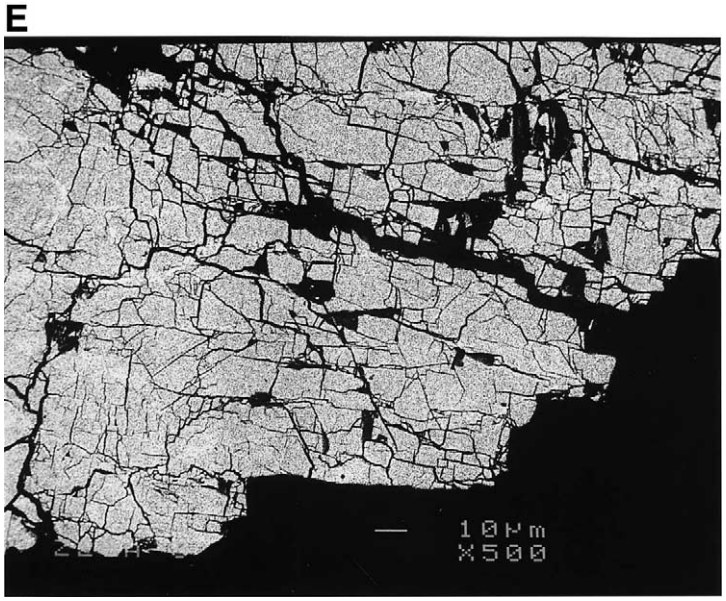

Fig. 2. Optical microscopic (A), SE (B), BSE (C), and CL (D) images of the 20 GPa zircon sample. The 20 GPa sample exhibits a high density of irregular fractures and a mosaic texture, which is also shown in a more magnified BSE image (E). D clearly shows the presence of the areas that have higher CL intensity (areas II as discussed in the text). The scale of (A) is the same as in (B).

formed to date. Here, we present the results of CL and backscattered electron (BSE) imaging, as well as of Raman spectroscopy performed on the experimentally shocked (shock pressures from 20 to 60 GPa) zircon specimens of [11]. The purpose of these measurements is to investigate the capability of the SEM–CL technique to document shock microdeformation effects and to determine whether CL and Raman characteristics of zircon could be indicative of particular shock pressure stages.

2. Experimental procedure

Two natural zircon crystals of about 1 cm length and 0.5 and 0.7 cm width from Australia (sample A) and from Sri Lanka (sample B), respectively, were experimentally shock-deformed, as described by Leroux et al. [11]. These authors investigated the shocked sample from Australia by TEM for the different types of induced shock deformation. The two large crystals had been cut into plates of about 1 mm thickness, perpendicular to their crystallographic *c*-axes. Shock recovery experiments were performed on such plates, which had been embedded in potassium iodide, using the shock reverberation technique at the Ernst-Mach-Institute, Germany (e.g., [10,13]). Carbon-coated, polished thin sections had then been produced from all samples. For the present study, polished thin sections, produced from the experimentally shocked plates of both zircon crystals, were utilized. All samples were examined with an Oxford mono-CL system attached to a JEOL JSM 6400 SEM. However, only the specimens from sample A were selected for further CL and Raman spectroscopic investigations because the sections were of better quality than those from sample B. Operating conditions for all SEM–CL investigations were 15 kV accelerating voltage and 1.2 nA beam current. CL spectra were recorded in the wavelength range of 200–800 nm with 1 nm wavelength steps. The grating of the monochromator was 1200 lines/mm. CL and BSE images were taken on Polaroid 4×5 instant film (ISO 800/30). Raman spectra were obtained with a Renishaw RM1000 confocal micro-Raman spectrometer with a 20 mW, 488 nm Ar

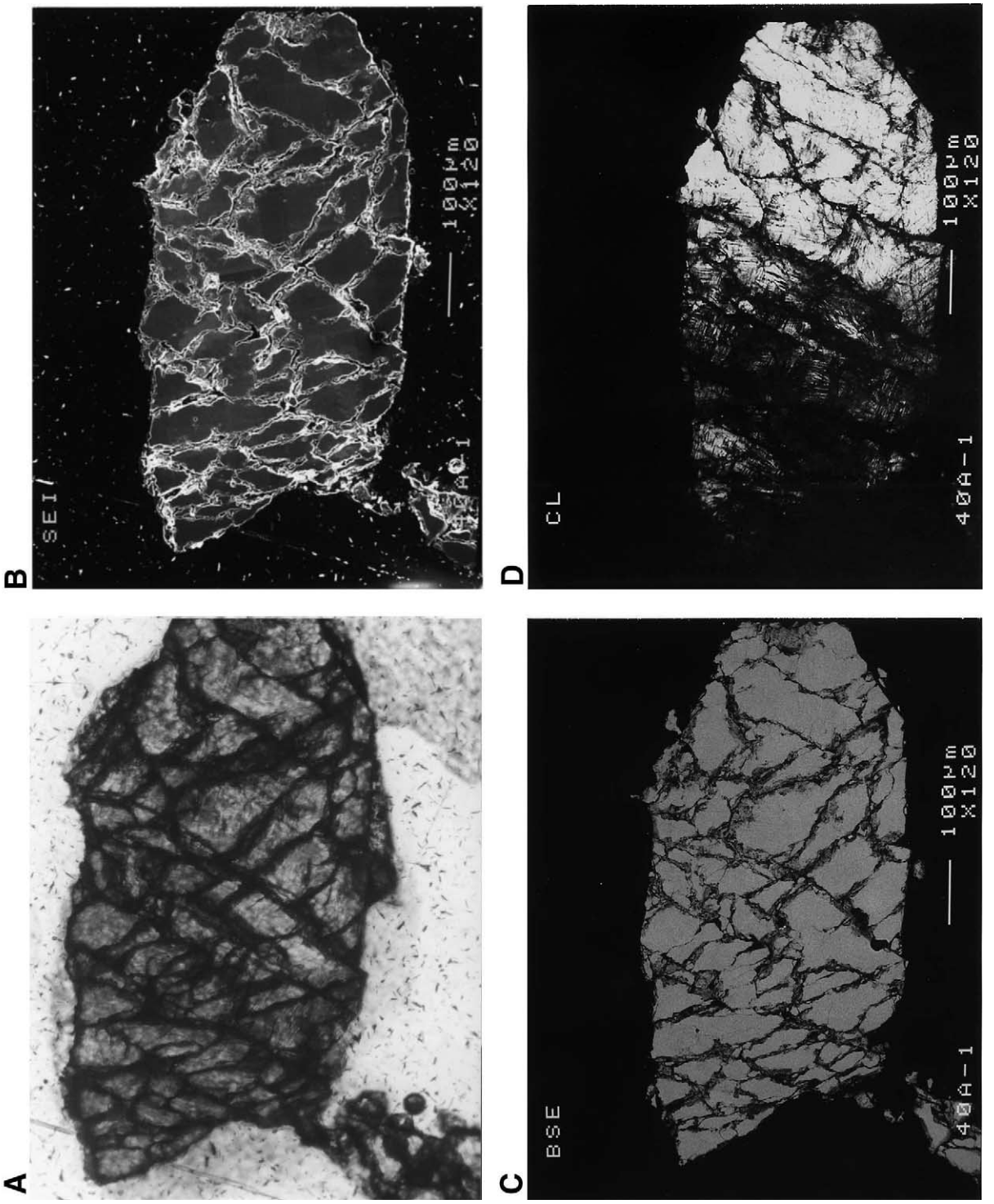
A
B
SEI
100μm
X120
40A-1
C
BSE
100μm
X120
40A-1
D
CL
100μm
X120
40A-1

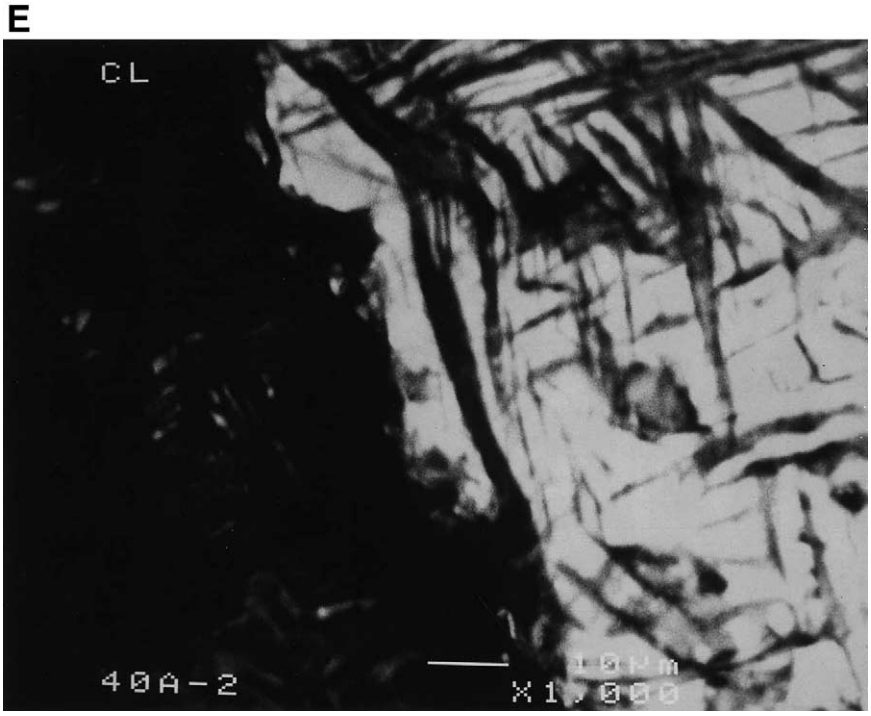

Fig. 3. Optical microscopic (A), SE (B), BSE (C), and CL (D) images of the 40 GPa sample. Some areas have distinctly higher CL intensities, as shown by the bright areas in CL images (D). A CL image (E) taken at high magnification exhibits a high density of well-developed (dark) lamellae, which are characteristic of this shock level. The scale of (A) is the same as (B).

ion laser excitation system and a thermo-electrically cooled CCD detector. Spectra were obtained in the range 100–1200 cm^{-1} with total exposure times of approximately 4 min. About 200×200 μm areas were selected for CL and BSE imaging. Raman spectra were taken from 3×3×3 μm^3 sample volumes and CL spectra were obtained from approximately 35×35 μm areas. In general, 10 CL spectra and three Raman spectra were acquired per specimen.

3. Results

3.1. BSE and CL images

3.1.1. Unshocked sample

The specimen of unshocked zircon is cut by open, irregularly shaped, fractures (Fig. 1A,B). Individual fractures have widths typically ranging from 5 to 25 μm. These fractures are easily visible in the BSE image (Fig. 1C). In addition, we observed that the unshocked grain displays a well-developed growth zonation parallel to the crystal edges. The widths of individual growth zones vary from 150 to 270 μm. The zones represent variations in BSE intensities. In some areas, the zircon contains patchy areas (Fig. 1C,D) exhibiting a distinct inverse relation between BSE and CL brightness.

3.1.2. 20 GPa sample

Compared to the undeformed sample, the fracture density of the 20 GPa specimen is significantly higher (Fig. 2A–C). Leroux et al. [11] reported the presence of ubiquitous microdeformation in these 20 GPa samples, including pervasive microcleavage parallel to {010} planes and dislocation patterns as distinguished by TEM. In the CL and BSE images of the present study (Fig. 2C,D), no planar microdeformations – of any type – are discerned. Many fractures are non-pla-

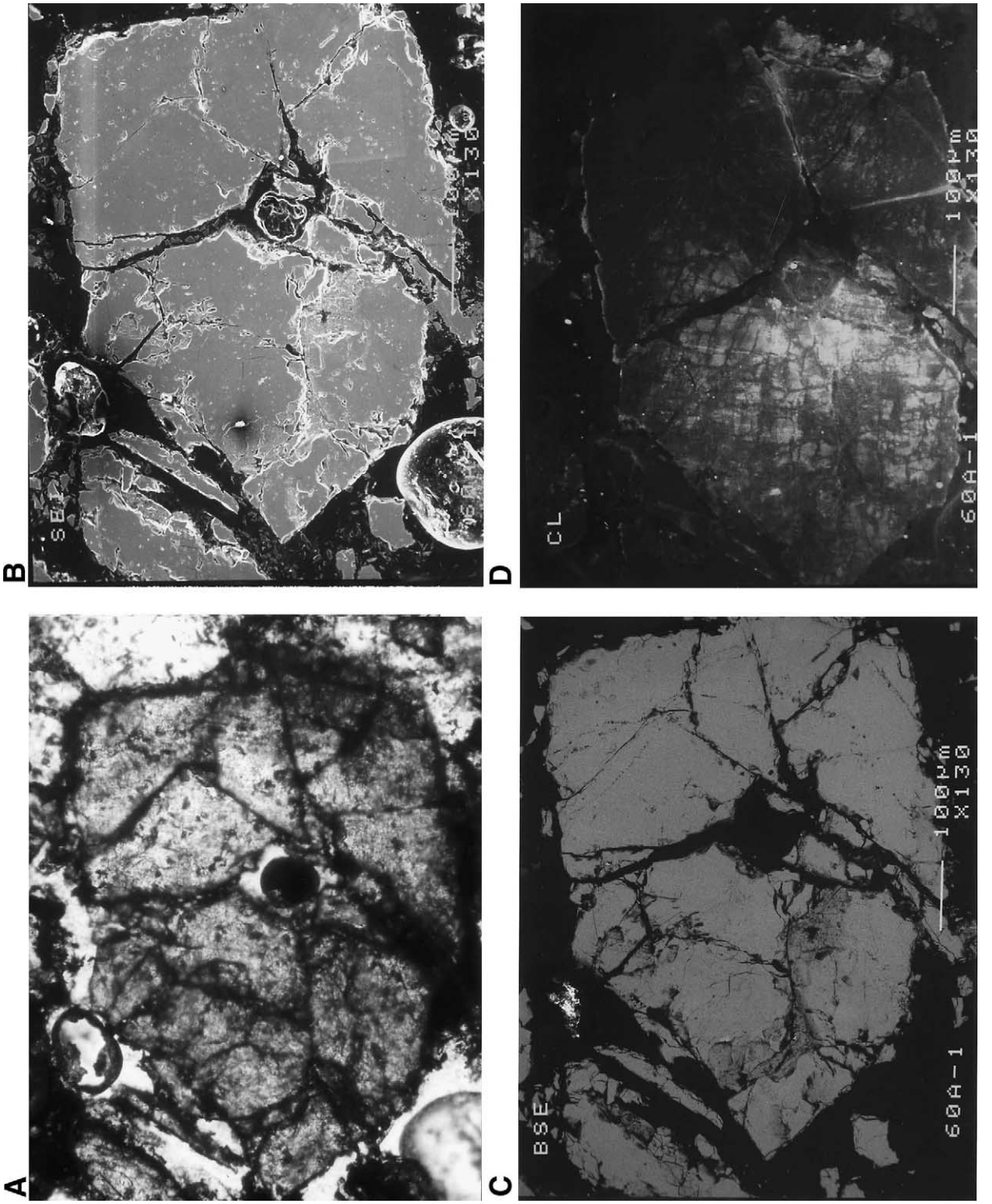
A
B
C
D
BSE
CL
60A-1
100μm
X130

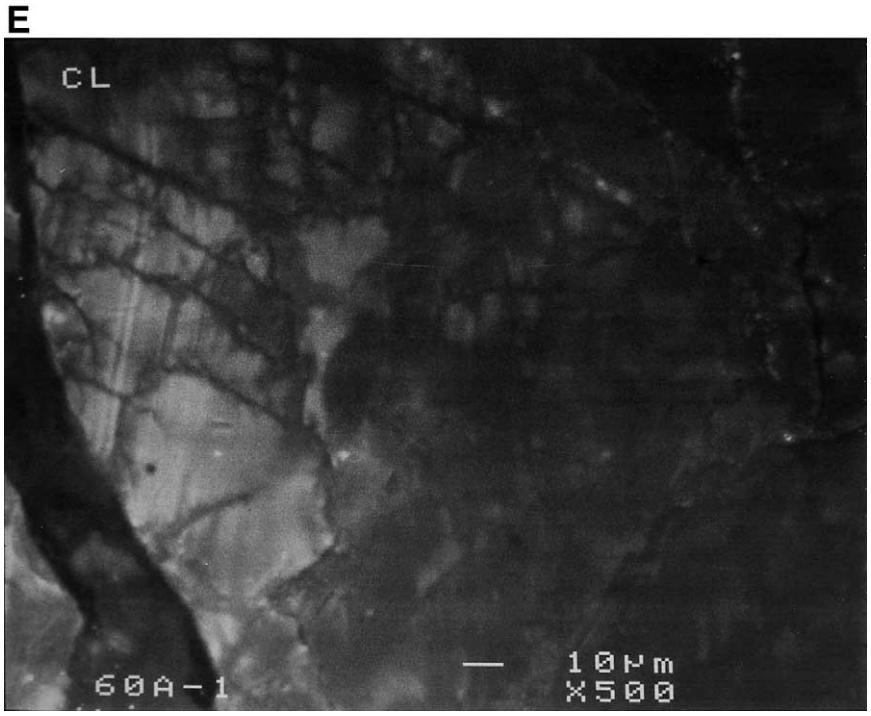

Fig. 4. Optical microscopic (A), SE (B), BSE (C), and CL (D) images of the 60 GPa sample. Relatively widely spaced (10–20 μm), grain-pervasive fractures are characteristic of this sample. The CL intensity is also rather low in the magnified CL image (E). The scale of (A) is the same as (B).

nar, but several distinct, apparently crystallographically controlled systems of semi-planar, cleavage-like fractures are visible, for example, in Fig. 2C (BSE). These fractures show a wide range of lengths and typical widths of 3–5 μm (Fig. 2E).

The CL image (Fig. 2D) of the 20 GPa sample shows irregularly distributed bright areas (about 10 μm across). The appearance of this uneven distribution of bright and dark areas resembles an optical shock-metamorphic effect known as 'shock mosaicism' [12,13].

3.1.3. 40 GPa sample

According to Leroux et al. [11], the 40 GPa sample consists of zircon that has been partially converted into the scheelite-type structure. PDFs of a glassy nature were observed by these authors in TEM images at the nm-scale in relics of zircon-structure material. One to several μm-wide microbands of the scheelite-structure phase could be found crosscutting material with zircon structure parallel to the {100} planes of zircon. According to [11], this displacive phase transformation showed the following relationships: $\{100\}_z$// $\{112\}_s$ and $[001]_z$//$[110]_s$.

Our BSE and CL images show that the 40 GPa sample is transected by a network of irregular fractures (Fig. 3A–C) that, locally, involve narrow zones of brecciation (Fig. 3E). This sample displays a high density of well-developed lamellae that are arranged in sets of narrowly spaced features, which are best visible in the CL images (Fig. 3E). These features (dark in the CL image) show a narrow range of widths (1–2 μm) and spacings (bright in the CL image) of 1–2 μm (Fig. 3E). In certain CL images (Fig. 3D,E), up to three sets of different orientations can be discerned. In contrast to the 20 GPa samples there is no mosaicism visible in the 40 GPa samples.

3.1.4. 60 GPa sample

The fracture densities observed in samples representing the lower shock stages are appreciably

higher than detected in the 60 GPa specimen (Fig. 4A,B). The irregular and crosscutting fractures in this sample have widths typically between 5 and 50 μm and are best visible in the BSE image (Fig. 4C). Leroux et al. [11] observed that the scheelite-structure phase is characterized by a high density of twins, as well as nm-scale PDFs oriented along {110} planes. Here, two types of microdeformations are observed. (1) In CL images, grain-pervasive, relatively widely spaced (10–20 μm), clearly subparallel, dark features are visible (Fig. 4E). (2) These features are set into a network of <3 μm wide features, which are shorter than the widely spaced ones, are also planar, often form crosscutting sets between pairs of the larger features (Fig. 4E), and are not visible in BSE images (Fig. 4C). Some of the 60 GPa sample grains exhibit very low CL intensities compared to the samples shocked at lower pressures (Fig. 4D).

3.2. CL spectrometry

Figure 5 shows a comparison of typical CL spectra for specimens representing the various shock stages. The unshocked sample exhibits four sharp emission lines at 314, 485 (triplet), 581, and 631 nm, and a broad band centered at 405 nm (Table 1; Fig. 5). Such intense peaks at about 485 and 580 nm have previously been described from zircon from Norwegian gneiss [1] and from synthetically doped (with REE activators: e.g., Tb^{3+}, Dy^{3+}, Tm^{3+}, etc.) zircon [3]. Position and shape of the broad band observed in the CL spectra of all of our samples are quite different from what has been described in previous CL studies of unshocked zircon. CL spectra of the embedding material (epoxy resin) and of the glass slide used for mounting the zircon grains show that these materials do not contribute to the broad bands observed in the zircon spectra of this study. The relative peak intensities show systematic changes between areas of bright and low luminescence in the CL images (Fig. 1D). The triplet emission line at 485 nm represents the strongest peak in all spectra obtained from the unshocked sample (Fig. 5 and Table 1).

In the 20 GPa sample, two types of CL spectra, corresponding to the two areas of different luminescence levels in CL images (Fig. 2D), can be distinguished. The darker areas (which dominate), are marked as type I in Figs. 5 and 6, and the rare brighter areas are marked as type II. The characteristics of these areas are as follows. (I) A broad band is centered at 405 nm, and narrow emission lines are at 314, 485 (triplet peak), 581, and 630 nm. (II) Four minor peaks at 315, 385, 406, and 419 nm are superimposed on a broad band centered at 334 nm. The narrow emission lines at 483 (triplet) and 580 nm exhibit relatively high intensities, whereas the peak at 630 nm is comparatively weak (20 GPa [II] in Fig. 5). An additional weak band appears at 548 nm (Fig. 5 and Table 1). In the bright luminescent regions of this

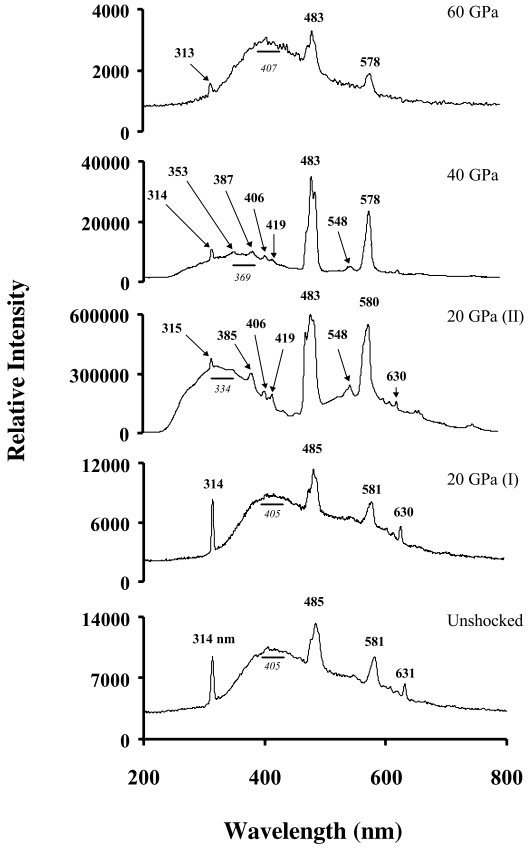

Fig. 5. CL spectra of unshocked and shocked (20, 40, and 60 GPa) zircon samples, showing sharp emission lines and broad bands in the near-UV and visible light range. Two types of CL spectra for the CL dark and bright areas in the 20 GPa sample (I and II, respectively) can be distinguished. Numbers denote peak positions in nm.

sample, the peak intensities of the narrow emission lines are significantly higher than in the dark areas (Fig. 2D and Table 1).

The CL spectra of the 40 GPa sample contain a broad band centered around 369 nm in the near-UV region. The spectra are, furthermore, characterized by two very strong emission lines at 483 (triplet) and 578 nm (Fig. 5). In addition, five weak emission centers at 314, 353, 387, 406, and 419 nm are superimposed on the broad band in the near-UV range. An additional weak band appears at 548 nm, which is also seen in the bright 20 GPa areas (II). In the bright luminescent regions (right side of Fig. 3E), the peak intensities of the sharp emission lines are higher than in the darker regions (left side of Fig. 3E).

The CL spectra of the 60 GPa sample show three sharp emission lines at 313, 483 (triplet), and 578 nm (Table 1). A broad band is centered at 407 nm. The peaks show lower peak intensities compared to the lower pressure samples (20 and 40 GPa; Fig. 5).

3.3. Raman spectroscopy

Raman spectra were obtained from all four

Table 1
Emission bands in CL spectra (obtained under identical measurement conditions) of unshocked and shocked (20, 40, and 60 GPa) zircon samples, including peak positions and relative peak intensities (minimum and maximum) of broad bands and sharp emission lines in the near-UV and visible light range

Shock pressure (GPa) [number of spectra]	Broad band (nm)	Sharp emission lines (nm)[a]	Minimum peak intensity (arbitrary units)	Maximum peak intensity (arbitrary units)
0	405		5 120	9 395
[6]		314	4 590	7 717
		485	6 380	13 247
		581	4 530	9 448
		631	2 790	6 290
20 (I)	405		4 200	8 730
[4]		314	4 450	8 580
		485	5 300	11 400
		581	3 946	8 090
		630	3 090	5 550
20 (II)	334		4 910	329 000
[2]		315	5 920	376 000
		385	4 970	299 000
		406	4 001	200 070
		419	3 520	195 000
		483	17 900	597 000
		548	3 890	242 000
		580	1 250	548 000
		630	5 920	376 000
40	369		3 320	12 300
[6]		314	3 370	12 900
		353	3 430	12 800
		387	3 550	13 100
		406	3 310	11 500
		419	3 120	9 600
		483	7 750	48 600
		548	2 700	5 950
		578	6 170	33 000
60	407		3 075	8 690
[5]		313	1 038	7 560
		483	1 545	10 565
		578	1 285	5 380

[a] Positions of emission lines vary slightly (±2 nm) between individual spectra.

specimens. We acquired three Raman spectra per sample. However, only one spectrum is shown in Fig. 6 for each sample, as the other spectra are identical. Intensity variations due to polarization effects were not observed, as all samples were excited at approximately 45° to the laser beam.

The Raman spectra of the unshocked, 20, 40, and 60 GPa zircon specimens are distinctly different. The unshocked sample exhibits one major peak at 999 cm^{-1}. In the 20 GPa sample, the two areas that had been distinguished by their different CL intensities (I and II) were also both analyzed by Raman spectroscopy. In both cases, the peak at about 1000 cm^{-1} is dominant. However, in contrast to the unshocked sample, the intensity of this peak is considerably lower in spectra from both areas. In addition, two peaks appear at 356 and 444 cm^{-1}. In general, spectra from both areas did not exhibit any significant differences. Only the background intensity (caused by luminescence) is higher in the spots that have higher CL intensity (II).

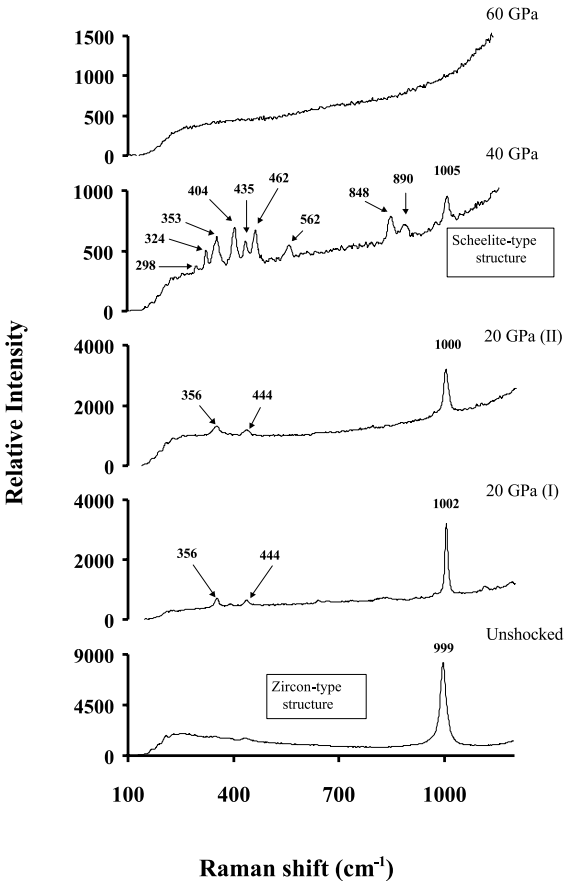

Fig. 6. Raman spectra of unshocked and shocked (20, 40, and 60 GPa) zircon samples, showing significant changes in the appearance of the spectra with different shock pressures. Whereas peaks of the unshocked and 20 GPa samples indicate zircon structure, the bands of the 40 GPa sample are characteristic of the high-pressure scheelite-type phase. The total absence of peaks in the spectrum of the 60 GPa sample indicates amorphization of this sample. Numbers denote peak positions in cm^{-1}.

The spectrum of the 40 GPa sample is dominated by a number of peaks at 298, 324, 353, 404, 435, 462, 562, 848, 890, and 1005 cm^{-1}. In contrast, the Raman spectra of the 60 GPa sample are characterized by the total absence of any peaks. Only a sloping background line is revealed, similar to that of the other samples (Fig. 6).

An additional Raman spectrum (available upon request from the corresponding author) was obtained from the 40 GPa sample with a total exposure time of approximately twelve hours. It yielded exclusively a scheelite-structure phase spectrum [23], but with improved signal-to-noise ratio.

4. Discussion

4.1. The nature of SEM–CL properties of phase transformation from zircon structure to the scheelite-type phase

The inverse relationship between BSE and CL brightness is readily explained. The BSE contrast in the zircon samples is sensitive to changes of average atomic number, i.e., higher Z, causing a higher BSE yield. In the case of natural zircon, higher concentrations of Hf, Y, Yb, U, and Th correspond to higher BSE intensities. In contrast, in the CL images, these elements cause low intensities as they cause quenching of the CL signal [2,20,21].

The CL spectra of the 20 GPa sample exhibit two different spectral types corresponding to the two areas of different luminescence brightness. This sample exhibits predominantly zircon-structure CL spectral properties. However, spectra ob-

tained on the CL bright type II areas resemble the CL spectral properties of the 40 GPa sample, which is interpreted to represent zircon relics in the scheelite-structure phase. This observation might indicate that the phase transformation from the zircon- to the scheelite-type structure begins in relatively small areas with enhanced CL brightness in the 20 GPa sample. It is important to note, however, that our Raman spectra of the 20 GPa sample did not indicate the presence of any areas composed of scheelite-structure phase.

The high density of narrowly spaced lamellae that are visible in the 40 GPa sample (especially in the CL images) might result from the zircon being converted to the scheelite-type structure phase [11]. The zircon- to scheelite-structure phase transition involves a significant volume decrease and changes in the *c*/*a* ratio, which is accompanied not by a change in primary coordination number of Si and Zr cations but only by rotation of the SiO_4 tetrahedra [20].

The Raman spectrum of the 60 GPa sample indicates that this sample is amorphous. The flat, broad bands and weak emission lines of the CL spectra are in good agreement with this observation. The weak, sharp CL emission lines at around 313, 483, and 578 nm are at positions equivalent to peaks observed for all other samples. As a consequence, the local environment of the luminescence centers, i.e., field strength, site symmetry, and coordination number, is similar in all cases. This indicates that these centers have not been redistributed even at the highest shock pressure of 60 GPa.

4.2. CL and Raman spectral properties of unshocked and shocked (20–60 GPa) zircon samples

In general, CL spectra of zircon are characterized by REE^{3+} centers, causing sharp emission peaks in the visible range [1–3]. In the present study, CL luminescence centers are dominated by Dy^{3+}, indicated by the relatively strong peaks at 478–487 and 573–586 nm. According to Blanc et al. [3], the two weak emission lines at 315 and around 628 nm might be assigned to Gd^{3+} (Fig. 5; Table 1). A weak band at 548 nm might be related to Tb^{3+} [3]. Broad emission bands are thought to be generally caused by lattice defects (J. Götze, personal communication, 2002). Therefore, the broad bands of CL spectra in the near-UV range are probably related to structural imperfections, such as shock damage, radiation damage, or poor ordering [1,21]. Electron defects at O in Ti–O or Zr–O systems, OH^- defects, and broken atomic bonds could also be related to broad bands in the near-UV range [21].

Raman spectra of natural zircon have been described by, e.g., Nasdala et al. [22]. Raman spectra of the high-pressure scheelite-type phase (obtained in static high-pressure experiments) have been reported by Knittle and Williams [23]. According to these authors, the peak at about 1003 cm^{-1} observed in all samples besides the 60 GPa sample is related to the SiO_4 antisymmetric stretching (v_3) vibration. The 20 GPa sample contains two additional, relatively significant vibrations at about 435 cm^{-1}, assigned to the SiO_4 bending (v_2) mode, and at 356 cm^{-1}, thought to represent a lattice mode. The peaks observed in the 40 GPa sample are in excellent agreement with previous studies on the scheelite-type phase [23]. The peaks at about 324 cm^{-1} (lattice mode), 848 cm^{-1} (strain activated mode), 890 cm^{-1} (v_3:SiO_4 antisymmetric stretching) [23] appear only in the 40 GPa sample (Fig. 6). It should be noted, however, that additional peaks occur at about 353, 435, and 1005 cm^{-1}. The peak positions of these modes are very similar to those characteristic of the zircon-structure phase (e.g., 20 GPa sample). Even if these features were also observed in the scheelite-type spectra of high-pressure zircon by Knittle and Williams [23], there is a high probability that minor amounts of relic zircon phase material are still present in the 40 GPa sample. This finding is in good agreement with the results of the TEM investigations by Leroux et al. [11], who did not observe single-phase scheelite-type material in the 40 GPa sample, but an epitaxial intergrowth of both phases with domain sizes below the spatial resolution of the micro-Raman spectrometer used in the present study.

In the 60 GPa sample, the extreme shock pressure has led to apparent amorphization of the scheelite-structure phase. None of the Raman

spectra collected from the 60 GPa specimen show any peaks. Therefore, it is likely that the high shock pressure caused complete structural disturbance with considerable displacement of atoms. This observation is contrary to the observations by Leroux et al. [11], who showed that the scheelite-type phase is a stable crystalline phase at 60 GPa. The transformation from zircon- to scheelite-type structure is displacive and, thus, rapidly achieved, and this phase is easily quenchable. The 60 GPa Raman signature would be compatible with preservation of SiO_4 tetrahedral units, but with a large inter-tetrahedral Si–O–Si angle distribution. However, at this stage, the nature of the CL signature of the 60 GPa sample cannot be fully ascertained.

In conclusion, the combination of BSE and CL imaging and CL and Raman spectroscopy is a potentially useful tool that can be used to characterize the shock stage of zircons from impactites. Further research, however, is required before an attempt can be made to sufficiently quantify these results to convert them into a functioning shock barometer for zircon. For instance, CL could be complemented by time-resolved photoluminescence investigations, which could help to accurately assign different luminescence lines to, e.g., different REEs. Our results also give new insight into the structural changes that occur in zircons during shock metamorphism, and the pressures associated with these changes.

Acknowledgements

We would like to thank Jens Götze and Ulf Kempe (University Freiberg, Germany) for helpful comments, and Gero Kurat (Natural History Museum, Vienna, Austria) for access to the SEM–CL facility at the Natural History Museum, Vienna, Austria. We are grateful to H. Dypvik and two anonymous reviewers for constructive and detailed comments on the manuscript. This work was supported by the Austrian Science Foundation, Grant Y58-GEO. WUR's contribution results from a short sabbatical stay at the University of Vienna, made possible by financial contributions from this institution as well as the National Research Foundation of South Africa. This paper represents Wits University Impact Cratering Research Group, Contribution No. 41.*[AC]*

References

[1] D.J. Marshall, Cathodoluminescence of Geological Materials, Unwin Hyman, Boston, 1988, 146 pp.
[2] C.L. Hayward, Cathodoluminescence of ore and gangue minerals and its application in the minerals industry, in: L.J. Cabri, D.J. Vaughan (Eds.), Modern Approaches to Ore and Environmental Mineralogy, Mineralogical Association of Canada, Short Course Series 27, 1978, pp. 269–325.
[3] P. Blanc, A. Baumer, F. Cesbron, D. Ohnenstetter, G. Panczer, G. Rémond, Systematic cathodoluminescence spectral analysis of synthetic doped minerals: anhydrite, apatite, calcite, fluorite, scheelite and zircon, in: M. Pagel, V. Barbin, P. Blanc, D. Ohnenstetter (Eds.), Cathodoluminescence in Geosciences, Springer, Berlin, 2000, pp. 127–160.
[4] S. Boggs, D.H. Krinsley, G.G. Goles, A. Seyedolali, H. Dypvik, Identification of shocked quartz by scanning cathodoluminescence imaging, Meteorit. Planet. Sci. 36 (2001) 783–793.
[5] G. Åberg, B. Bollmark, Retention of U and Pb in zircons from shocked granite in the Siljan impact structure, Sweden, Earth Planet. Sci. Lett. 74 (1985) 347–349.
[6] B.F. Bohor, W.J. Betterton, T.E. Krogh, Impact-shocked zircons: discovery of shock-induced textures reflecting increasing degrees of shock metamorphism, Earth Planet. Sci. Lett. 119 (1993) 419–424.
[7] T.E. Krogh, W.D. Davis, F. Corfu, Precise U–Pb zircon and baddeleyite ages for the Sudbury area, in: E.G. Pye, A.J. Naldrett, P.E. Giblin (Eds.), The Geology and Ont. Geol. Surv. Spec. 1, 1984, pp. 431–446.
[8] S.L. Kamo, T.E. Krogh, Chicxulub crater source for shocked zircon crystals from the Cretaceous–Tertiary boundary layer, Saskatchewan: evidence from new U–Pb data, Geology 23 (1995) 281–284.
[9] B.P. Glass, S. Liu, Discovery of high-pressure $ZrSiO_4$ polymorph in naturally occurring shock-metamorphosed zircons, Geology 29 (2001) 371–373.
[10] A. Deutsch, U. Schärer, Isotope systematics and shock-wave metamorphism. I. U–Pb in zircon, titanite, and monazite, shocked experimentally up to 59 GPa, Geochim. Cosmochim. Acta 54 (1990) 3427–3434.
[11] H. Leroux, W.U. Reimold, C. Koeberl, U. Hornemann, J.-C. Doukhan, Experimental shock deformation in zircon: a transmission electron microscopic study, Earth Planet. Sci. Lett. 169 (1999) 291–301.
[12] B.M. French, Traces of Catastrophe: A Handbook of Shock-Metamorphic Effects in Terrestrial Meteorite Im-

pact Structures, LPI Contribution No. 954, Lunar and Planetary Institute, Houston, 1998, 120 pp.
[13] D. Stöffler, F. Langenhorst, Shock metamorphism of quartz in nature and experiment. I. Basic observation and theory, Meteoritics 29 (1994) 155–181.
[14] R.A.F. Grieve, F. Langenhorst, D. Stöffler, Shock metamorphism of quartz in nature and experiment. II. Significance in geosciences, Meteorit. Planet. Sci. 31 (1996) 6–35.
[15] W.U. Reimold, H. Leroux, R.L. Gibson, Shocked and thermally metamorphosed zircon from the Vredefort impact structure, South Africa: a transmission electron microscopic study, Eur. J. Mineral. (2002) (in press).
[16] S.L. Kamo, W.U. Reimold, T.E. Krogh, W.P. Colliston, A 2.023 Ga age for the Vredefort impact event and first report of shock metamorphosed zircons in pseudotachylitic breccias and Granophyre, Earth Planet. Sci. Lett. 144 (1996) 369–387.
[17] E. Deloule, M. Chaussidon, B.P. Glass, C. Koeberl, U–Pb isotopic study of relict zircon inclusions recovered from Muong Nong-type tektites, Geochim. Cosmochim. Acta 65 (2001) 1833–1838.
[18] B. Kleinmann, The breakdown of zircon observed in the Libyan Desert Glass as evidence of its impact origin, Earth Planet. Sci. Lett. 5 (1969) 497–501.
[19] K. Kusaba, Y. Syono, M. Kikuchi, K. Fukuoka, Shock behaviour of zircon: phase transition to scheelite structure and decomposition, Earth Planet. Sci. Lett. 72 (1985) 433–439.
[20] G. Koschek, Origin and significance of the SEM cathodoluminescence from zircon, J. Microsc. 171 (1993) 223–232.
[21] U. Kempe, T. Gruner, L. Nasdala, D. Wolf, Relevance of cathodoluminescence for the interpretation of U–Pb zircon ages, with an example of an application to a study of zircons from the Saxonian Granulite Complex, Germany, in: M. Pagel, V. Barbin, P. Blanc, D. Ohnenstetter (Eds.), Cathodoluminescence in Geosciences, Springer, Berlin, 2000, pp. 415–455.
[22] L. Nasdala, G. Irmer, D. Wolf, The degree of metamictization in zircon: a Raman spectroscopic study, Eur. J. Mineral. 7 (1995) 471–478.
[23] E. Knittle, Q. Williams, High-pressure Raman spectroscopy of $ZrSiO_4$: observation of the zircon to scheelite transition at 300 K, Am. Mineral. 78 (1993) 245–252.